Statistical analysis of the association between rheological properties of blood and atherosclerosis

M.Abbasian[1], M. Shams[1,*], Z. Valizadeh[1], A.r Moshfegh[2,3], A. Javadzadegan[2,3]

[1] Faculty of Mechanical Engineering, K. N. Toosi University of Technology, Tehran, Iran
[2] Faculty of Medicine and Health Sciences, Macquarie University, Sydney, NSW 2109, Australia
[3] ANZAC Research Institute, The University of Sydney, Sydney, NSW 2139, Australia

ABSTRACT: The aim of this study is to investigate the effects of non-Newtonian blood rheology models on the wall shear stress (WSS) distribution in a cohort of patients-specific coronary arteries. Twenty patients with diseased left anterior descending (LAD) coronary arteries (with varying degrees of stenosis severity from mild to severe) who underwent angiography and in-vivo pressure measurements were selected to perform computational fluid dynamics (CFD) simulations. Three-dimensional (3D) patient-specific geometries were reconstructed from 3D quantitative coronary angiography. To compare the effects of rheological properties of blood on WSS along the arteries, each artery was divided into 3 segments; proximal (pre-stenosis), stenosis and distal (post-stenosis). Blood was modelled as a Newtonian and non-Newtonian (Carreau-Yasuda, Casson and Power-law) fluid.
Our findings showed that the WSS distributions over proximal and stenosis segments were significantly affected by the non-Newtonian properties of blood whereas the effect was negligible over distal segment. On the other hand, the type of non-Newtonian model is important to achieve accurate results over proximal and stenosis regions, but over distal region, it does not matter what model is used. Therefore, to simplify the simulation, the Newtonian model can be acceptable in finding the wall shear stress distribution over the distal region regardless of severity of stenosis.

1. Introduction

Coronary artery atherosclerosis is the leading cause of mortality and morbidity in the world [1]. Because of its essential role in the development and progression of atherosclerosis, haemodynamics has become a fundamental tool in assessing functional significance of coronary arteries [2-4]. A comprehensive haemodynamic assessment of coronary arteries remains a non-trivial procedure, even with state-of-the-art medical imaging devices and analysis software [5]. Recent advances in medical imaging, computational power and mathematical algorithms enabled the previously challenging field of patient-specific computational fluid dynamics (CFD) to become a viable emerging tool for studying and understanding coronary haemodynamics in detail [2, 3, 6, 7].

The most important haemodynamic force is wall shear stress (WSS) exerted on the monolayer of endothelial cells lining the inside of the artery wall. It is imperative to study the rheological behaviour of blood and determine whether it is Newtonian or non-Newtonian, as this has a significant effect on WSS. In healthy arteries, at low shear rates (< 100 s^{-1}) blood behaves like a non-Newtonian fluid [8-10] whereas at high shear rates (> 100 s^{-1}), it can be treated as a Newtonian

fluid [10, 11]. However, when it comes to diseased arteries, there is no rule of thumb when blood should be treated as a Newtonian or non-Newtonian fluid.

Significant research has been carried out to determine haemodynamic effects of non-Newtonian properties of blood in healthy and diseased coronary arteries [12-17]. However, the common limitation of these studies is that they evaluated non-Newtonian characteristic of blood on a case by case basis, not in a cohort of coronary arteries with varying degrees of stenosis. Therefore, this has left an important research question unaddressed and that is whether there is a correlation between severity of coronary artery disease (CAD), degree of blood's non-Newtonian behaviour and haemodynamic perturbations. This study aims to address this by performing patient-specific CFD simulations in a cohort of 20 patients with varying degrees of CAD.

2. Methods

2-1- Patient selection

In this study, 20 patients with a stenosis in their left anterior descending (LAD) coronary arteries were included. Stenosis severity varied from 30% to 70% in the whole cohort. The stenosis severity was defined based on diameter stenosis percentage, as previous described [9]. Table 1 shows some clinical characteristic of the patients.

*Corresponding author's email: Shams@Kntu.ac.ir

Table 1. Baseline clinical characteristics of cohort of patients

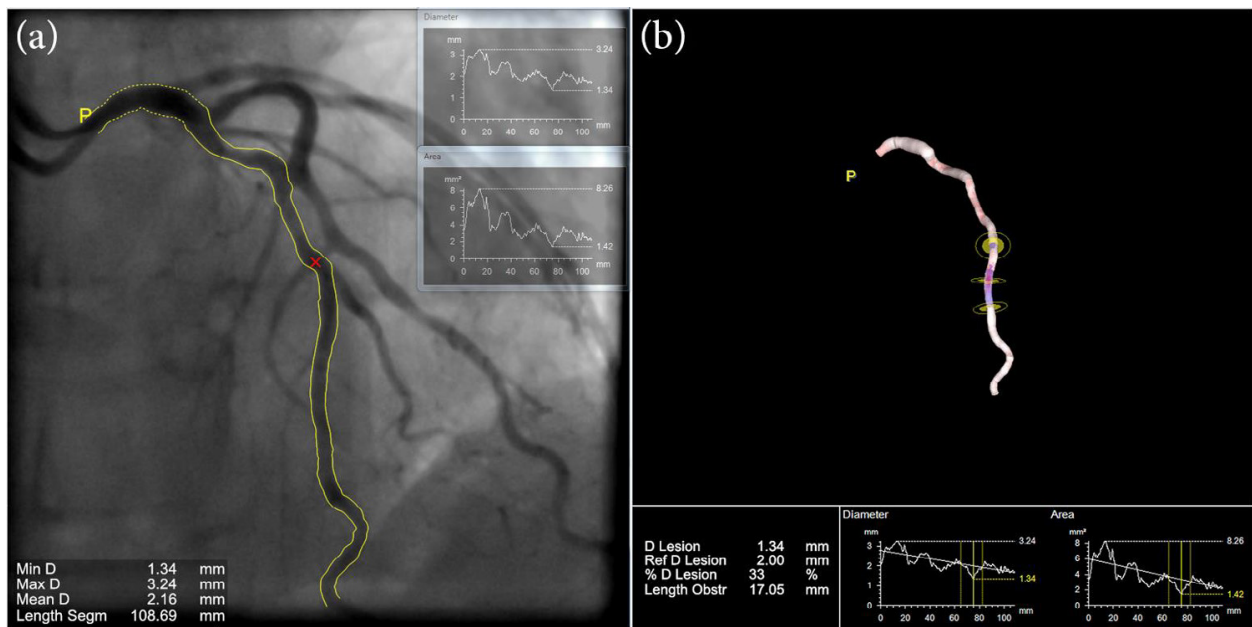| Variable	Value
Age, mean - year	63 ± 9
Male sex – no (%)	12 (60%)
Minimum lumen diameter (mm)	1.44 ± 0.35
Vessel size (mm)	2.99 ±0.42
Diameter stenosis percentage (%DS)	52.8 ± 18.4
Lesion length (mm)	10.6 ± 7.9
Resting proximal pressure (mmHg)	102 ± 17
Resting distal pressure (mmHg)	77 ± 15
Hyperaemic proximal pressure (mmHg)	89 ± 11
Hyperaemic distal pressure (mmHg)	58 ± 14
FFR	0.65 ± 0.25

Fig. 1. Reconstruction of geometry of a sample model (a) Coronary angiography of stenosed artery (LAD) of patient with geometric data (b) 3D reconstruction of stenosed artery. Location of the stenosis can be seen from diameter and area plots along the length of the artery very well.

2-2- Reconstruction of three-dimensional models of coronary arteries

Three-dimensional quantitative coronary angiography (3DQCA) was used to create the 3D LAD geometries of patients, using an in-house developed software utilizing state-of-the-art image processing and segmentation techniques [2].

Table 2. Equations of different blood viscosity models and their parameters

	Model	Effective viscosity equation	Parameters
1	Newtonian	$\mu = \mu_\infty$	$\mu_\infty = 3.45\,\text{mpa.s}$
2	Carreau-Yasuda [18]	$\mu = \mu_\infty + (\mu_0 - \mu_\infty)[1 + (\lambda\gamma)^q]^{\frac{n-1}{q}}$	$\mu_0 = 56\,\text{mpa.s},\ n = 0.22,\ q = 1.25$ $\mu_\infty = 3.45\,\text{mpa.s},\ \lambda = 1.902\,\text{s}$
3	Casson [19]	$\mu = (\sqrt{\mu_c} + \sqrt{\tau_c / \gamma})^2$	$\mu_c = 4.14\,\text{mpa.s},\ \tau_c = 3.80\,\text{mpa}$
4	Power-law [18]	$\mu = \mu^* \gamma^{n-1}$	$\mu^* = 35.00\,\text{mpa.s}^n,\ n = 0.6$

Fig. 1 shows an example of these models.

2-3- CFD Modelling

In order to perform CFD simulation of Newtonian and three non-Newtonian blood flow in stenosed arteries, ANSYS CFX 16 (ANSYS, Inc., Canonsburg, PA, USA) was used. Blood flow was assumed to be laminar, steady state, single phase and incompressible. The Newtonian model and three non-Newtonian models including Carreau-Yasuda, Casson, and Power-law were used to simulate the blood viscosity. The effective viscosity equations of blood and their parameters are presented in Table 2 in detail.

The Navier-Stokes equations (Equations (1), (2)) were used to simulating the blood flow under the mentioned assumptions.

$$\rho(\mathbf{u}.\nabla)\mathbf{u} = -\nabla p - \nabla.\boldsymbol{\tau} \tag{1}$$

$$\nabla.\mathbf{u} = 0 \tag{2}$$

Where u, ρ, p and τ are velocity vector, density of blood, static pressure and shear stress, respectively.

Arterial walls were assumed as a rigid boundary. No slip boundary condition was applied on the wall of the arteries. Average proximal and distal pressures, measured in vivo, were used as inlet and outlet boundary conditions, respectively.

Finite volume method was applied on numerical simulating. Governing equations were discretized based on first-order-upwind scheme. Convergence was achieved when the residuals of mass and momentum equations were less than 10^{-4}.

2-4- Grid generation

3D reconstructed geometries were meshed in ANSYS Meshing using tetrahedral elements. Fig. 2 shows an example of the utilized non-structured grid in the artery shown in Fig. 1.

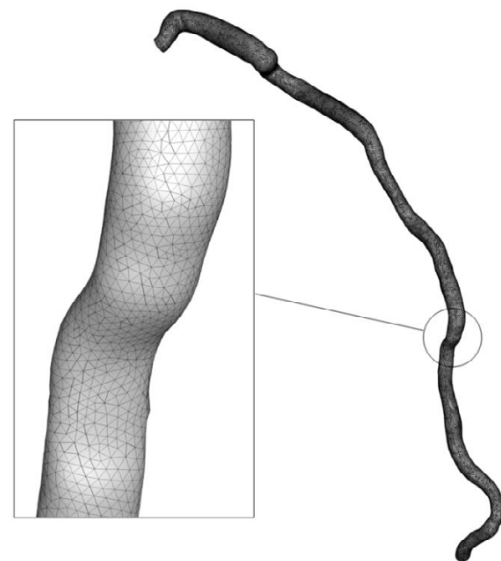Mesh independency was examined for all geometries. To achieve results without grid errors, the best size of the grid

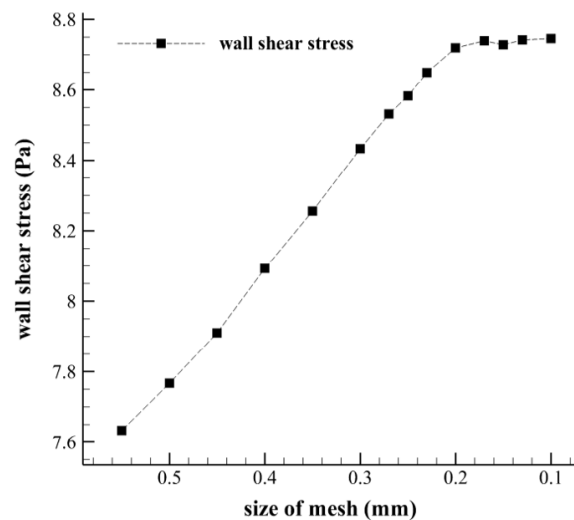**Fig. 2. Non-structured computational meshes of artery shown in Fig. 1**

Fig. 3. Grid independency test for artery shown in Fig. 1. The Figure shows the variation of wall shear stress magnitude (Pa) of single point on artery with respect to grid size (mm).

was selected. Fig. 3 shows the mesh dependency test for the artery shown in Fig. 1. As shown in this Fig., the best mesh size is 0.2 mm.

2-5- Statistical analysis

To determine if the difference between parameters of Newtonian and non-Newtonian models is statistically significant, T-tests were performed using Graph Pad Prism v. 7.01 (Graphpad, La Jolla, California). Resulted P-value less than 0.05 was considered as a significant difference.

3. Results

Figs. 4-6 show the contours of apparent viscosity for three arteries as a representation of various arteries including mild, moderate and severe stenosis sizes, for Carreau-Yasuda, Casson and Power-law models, respectively. It is notable that the mean diameters of the mentioned arteries are equal to 2.16 mm, 2.03 mm and 1.99 mm, respectively. In order to obtain a better comparison of different models, Figs. 4-6 indicate the percentage difference in dynamic viscosity between the non-Newtonian and Newtonian models. In the following contours, the arteries are divided into three regions. Region (1) is the proximal region which is from the inlet of the artery up to 20 mm before of the stenosis location. Region (2) is the stenosis region which contains ±20 mm of lesion point and region (3) is a distal region which is from 20 mm after stenosis location up to the end of the artery. In each region, the average value of dynamic viscosity (top panel) and the percentage difference (bottom panel) is specified. Also, the maximum and minimum value of viscosity and percentage difference in each artery is shown in the Figs. 4-6.

Results show that in all cases, the magnitude of dynamic viscosity varies along the arteries and it reduces significantly at the stenosis location. Therefore, we can infer that the minimum magnitude of dynamic viscosity occurs at the point of stenosis. There is reasonable evidence to support that in non-Newtonian models, the average of dynamic viscosity and its percentage difference between Newtonian and non-Newtonian models over distal region are almost less than two other regions. As an example, for the represented artery with a mild stenosis (Fig. 4), the average of dynamic viscosity over distal region, using the non-Newtonian Carreau-Yasuda model is 0.0039 Pa.s which is 12.34% greater than the Newtonian model. However, the average percentage difference in dynamic viscosity between non-Newtonian (Carreau-Yasuda) and Newtonian models over stenosis and proximal regions are about 13.91% and 25.47% respectively. Considering the variations of dynamic viscosity and its corresponding difference between various models in all patients, the maximum and the minimum of the percentage difference often occur at places where the magnitude of dynamic viscosity is maximum and minimum, respectively.

In the same way, the contours of WSS for three representation arteries are presented for all Newtonian and non-Newtonian models in Figs. 7-9. The WSS distribution

in each case varies and it is because of different geometries, different boundary conditions, and different viscosity models of the individual cases. Although WSS distribution is different between various arteries, the behavior of it over the stenosis region was found to be the same. In all cases, the magnitude of WSS increases suddenly at the throat of stenosis in each artery as shown in Figs. 7-9 (red areas in WSS contours).

As demonstrated in Figs. 7-9 (bottom panel), there are some differences in WSS magnitude between Newtonian and non-Newtonian models through each artery, which it changes in different areas from very low to very high amounts, however the average amount is almost low. Also, there are merit to suggest that in each artery where the WSS amount is low, the percentage difference is high, and the maximum difference often occurs at occasions that the magnitude of WSS is at minimum.

Tables 3-5 present the location of stenosis and also average of WSS over proximal, stenosis and distal regions for all twenty patients with mild, intermediate and severe lesions.

Figs. 10-12 show Variation of the average of WSS, dynamic viscosity and cross-sectional area of three represented arteries, along the length of the arteries for all Newtonian and non-Newtonian models. As shown in these Figures, both WSS and dynamic viscosity magnitude change with arterial cross-sectional variations. The average of WSS increases by decreasing the cross-section and on the contrary decreases by increasing it. But the average of dynamic viscosity for non-Newtonian models is completely opposite. It increases and decreases by increasing and decreasing the cross-sectional area, respectively. The magnitude of WSS increases suddenly at the throat of stenosis in each artery which can be seen as local peak point on WSS curves in the stenosis region. Unlike the WSS, the average of dynamic viscosity decreases suddenly at the throat of stenosis which its magnitude depends on the hemodynamic models. Dynamic viscosity curves along the artery express the stated contents clearly. As shown in Figs. 10-12, Power-law model has the widest range of dynamic viscosity among examined models. For example, for the represented mild artery, the average of dynamic viscosity varies from 0.0023 to 0.0067 Pa.s. However, the Carreau-Yasuda and Casson models give it from 0.0037 to 0.0050 Pa.s and 0.0044 to 0.0053 Pa.s, respectively. Observations show that almost when the average of WSS is relatively small (proximal region), resulted WSS using Newtonian model is less than resulted WSS using Power-law model and when the average of WSS is relatively high (distal region), Newtonian model gives the average of WSS along the artery greater than Power-law model.

Fig. 13 presents the T-test of WSS magnitude for all cases over three different regions. Comparing resulted P-values show that there is no statistically significant difference in WSS between Newtonian and non-Newtonian models over the distal region (P=0.0643>0.05). It means that in order to simplify simulation and probably reduce the time of solution, we can use the Newtonian model instead of non-Newtonian models over the distal region without significant changes in the WSS results. It can be applied to LAD coronary arteries including different stenosis sizes.
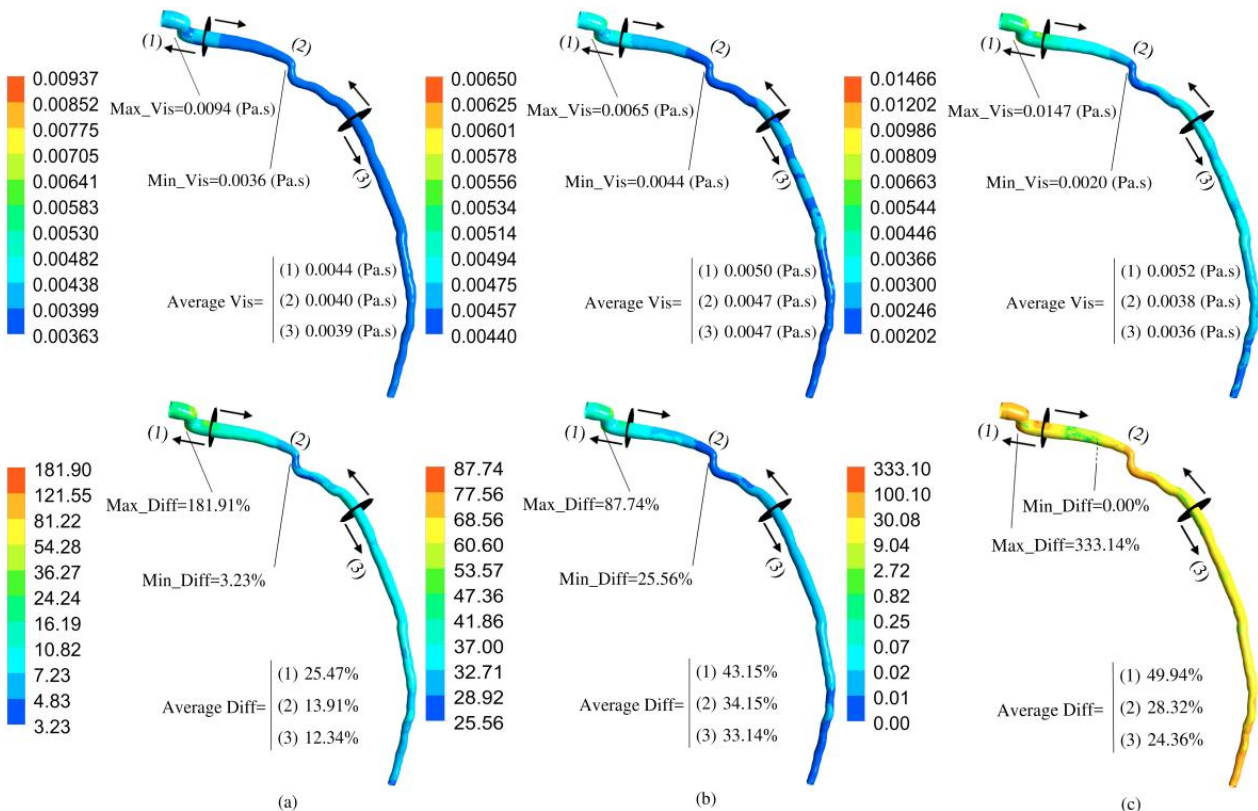
Fig. 4. Contours of dynamic viscosity magnitude distribution (top panel) and its percentage difference between Newtonian and non-Newtonian models (Bottom panel) for a representative patient-specific coronary artery with mild stenosis. (a) Carreau-Yasuda model, (b) Casson model and (c) Power-law model.
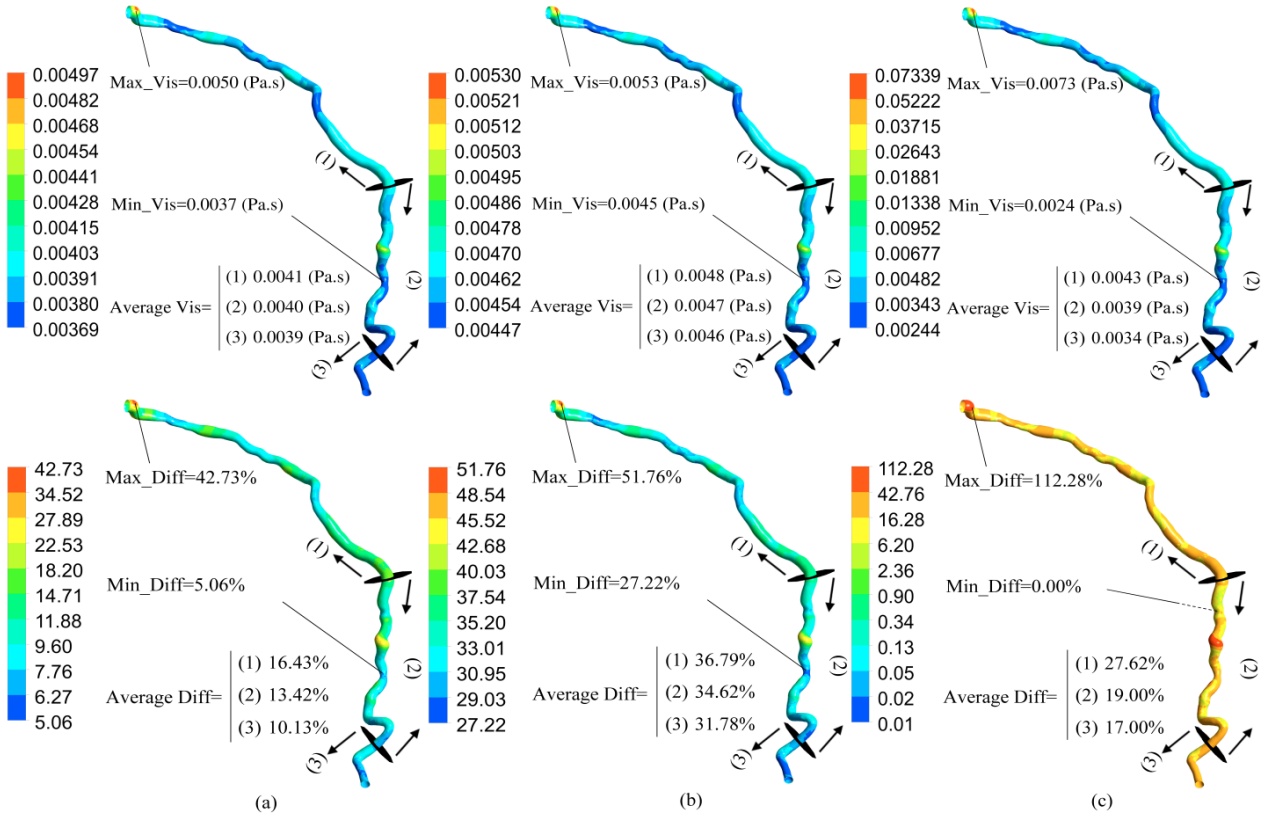

Fig. 5. Contours of dynamic viscosity magnitude distribution (top panel) and its percentage difference between Newtonian and non-Newtonian models (Bottom panel) for a representative patient-specific coronary artery with intermediate stenosis. (a) Carreau-Yasuda model, (b) Casson model and (c) Power-law model.
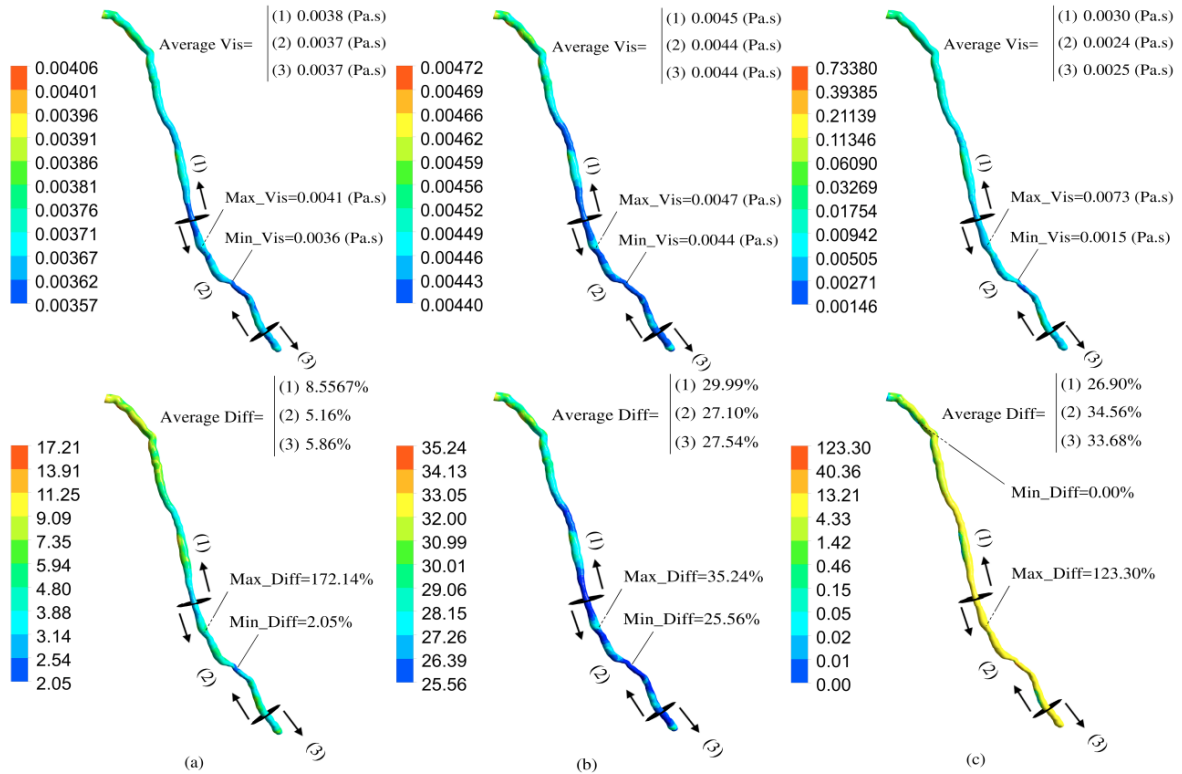
231

Fig. 6. Contours of dynamic viscosity magnitude distribution (top panel) and its percentage difference between Newtonian and non-Newtonian models (Bottom panel) for a representative patient-specific coronary artery with severe stenosis. (a) Carreau-Yasuda model, (b) Casson model and (c) Power-law model.
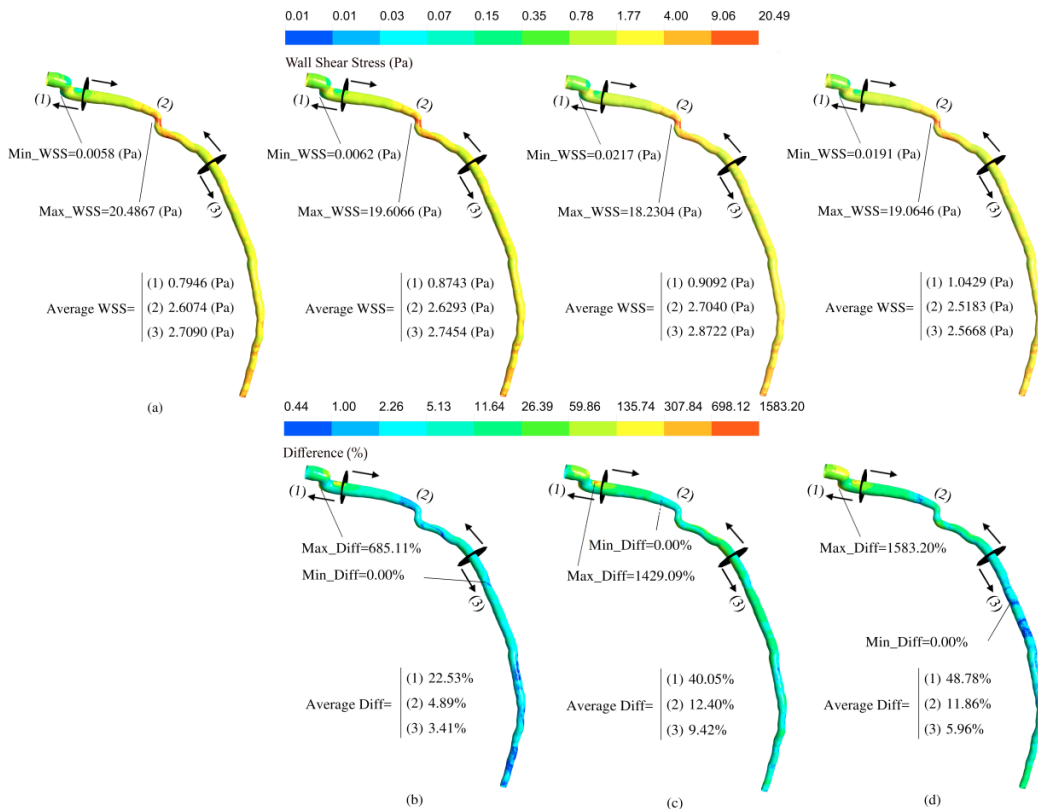

Fig. 7. Contours of WSS magnitude distribution (top panel) and its percentage difference between Newtonian and non-Newtonian models (Bottom panel) for a representative patient-specific coronary artery with mild stenosis. (a) Newtonian model, (b) Carreau-Yasuda model, (c) Casson model and (d) Power-law model.

Fig. 8. Contours of WSS magnitude distribution (top panel) and its percentage difference between Newtonian and non-Newtonian models (Bottom panel) for a representative patient-specific coronary artery with moderate stenosis. (a) Newtonian model, (b) Carreau-Yasuda model, (c) Casson model and (d) Power-law model.
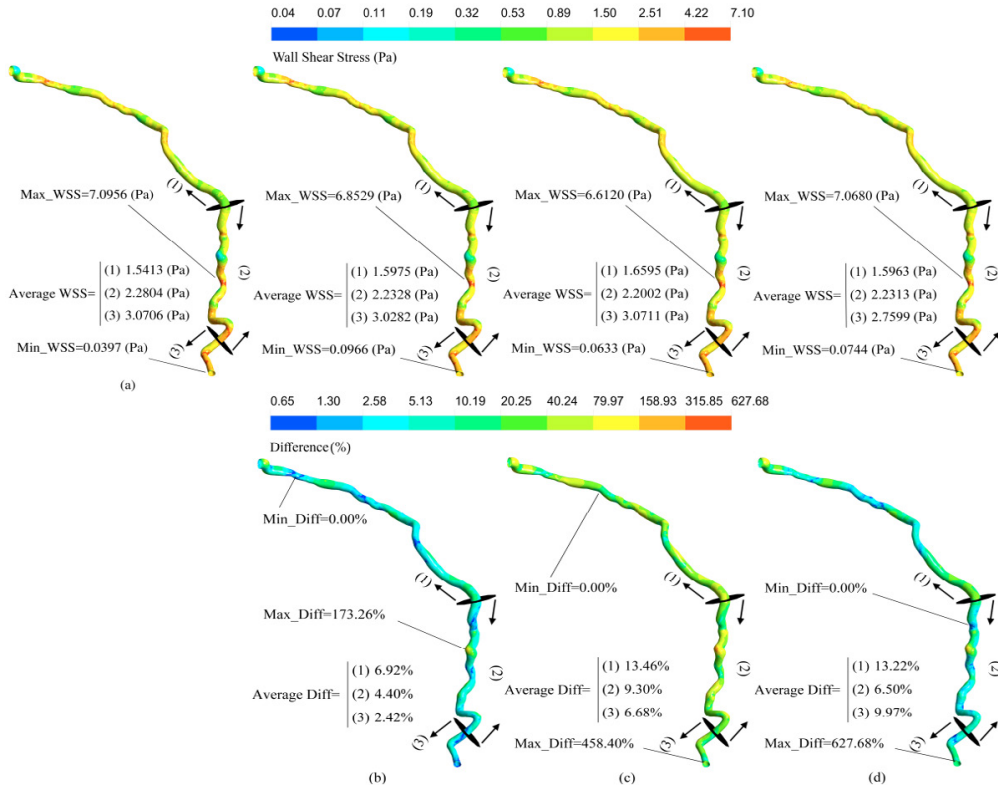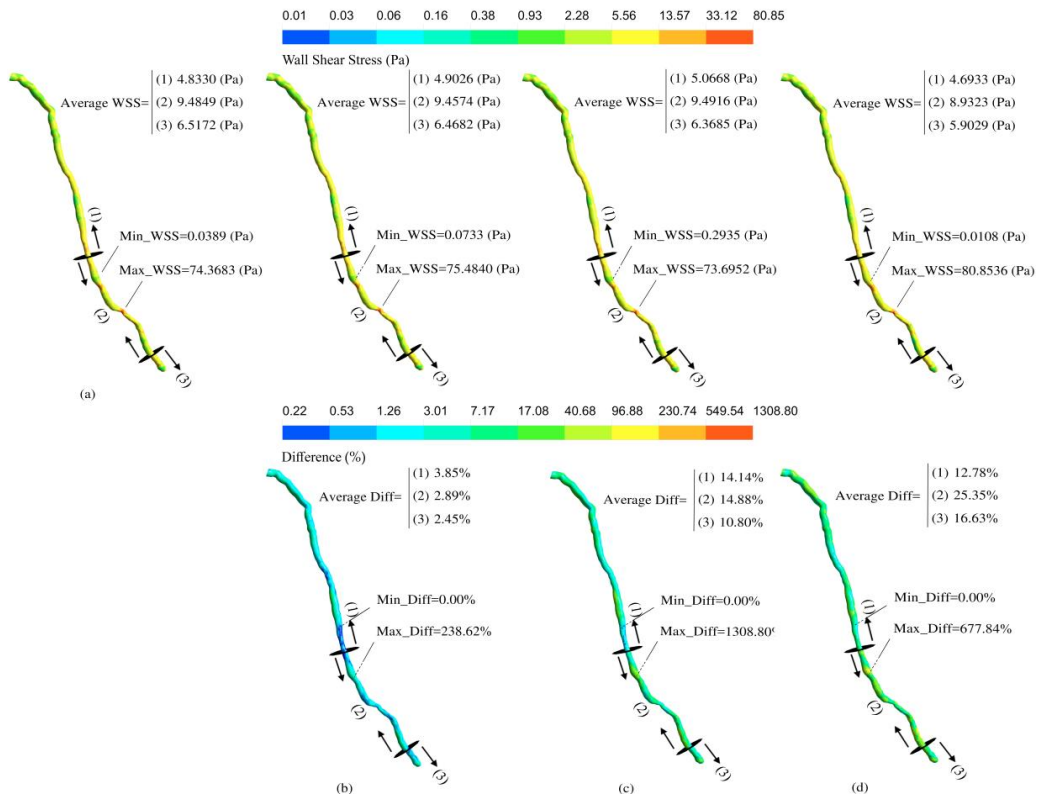

Fig. 9. Contours of WSS magnitude distribution (top panel) and its percentage difference between Newtonian and non-Newtonian models (Bottom panel) for a representative patient-specific coronary artery with severe stenosis. (a) Newtonian model, (b) Carreau-Yasuda model, (c) Casson model and (d) Power-law model.

Table 3. The location of stenosis and the average WSS over different regions along the artery with mild stenosis

Name	Model	Location of max stenosis centre from inlet (mm)	Average of WSS over proximal region (Pa)	Average of WSS over stenosis region (Pa)	Average of WSS over distal region (Pa)
Patient 1	Newtonian	111.1000	0.1673	1.3168	-
	Carreau-Yasuda		0.2291	1.2772	-
	Casson		0.2090	1.3007	-
	Power-law		0.3158	1.2217	-
Patient 2	Newtonian	74.2753	2.8182	5.2522	8.1500
	Carreau-Yasuda		2.8696	5.2689	8.0692
	Casson		2.9227	5.4448	7.8591
	Power-law		2.9416	4.9552	7.7934
Patient 3	Newtonian	29.0145	0.2192	0.3139	2.6879
	Carreau-Yasuda		0.3099	0.4154	2.7939
	Casson		0.3171	0.5130	2.9432
	Power-law		0.5087	0.6112	2.5935
Patient 4	Newtonian	31.3929	0.7946	2.6074	2.7090
	Carreau-Yasuda		0.8743	2.6293	2.7454
	Casson		0.9092	2.7040	2.8722
	Power-law		1.0429	2.5183	2.5668
Patient 5	Newtonian	119.9551	0.5102	3.2511	-
	Carreau-Yasuda		0.5713	3.1760	-
	Casson		0.5739	3.1966	-
	Power-law		0.7166	2.8637	-
Patient 6	Newtonian	25.0504	1.6186	1.9474	3.8807
	Carreau-Yasuda		1.7197	2.0326	3.9162
	Casson		1.7930	2.1229	4.0756
	Power-law		1.8940	2.0945	3.5429
Patient 7	Newtonian	110.1320	3.3472	9.0517	-
	Carreau-Yasuda		3.3924	8.9412	-
	Casson		3.4982	8.9284	-
	Power-law		3.3361	8.2414	-

Fig. 14 presents the T-test of maximum and minimum values of WSS along the arteries for all three sets of lesion size. It shows that all models give the minimum and maximum values of WSS without a statistically significant difference (P >0.05). In addition, as shown in Fig. 15, they predict the location of the maximum and minimum values of WSS along the arteries with an ignorable difference, too.

4. Discussion

Blood dynamic viscosity within the coronary arteries plays an important role in the behavior of atherosclerosis disease. For instance, it is known that any factor which increases the dynamic viscosity of blood, such as diabetes, hyperlipidemia, and smoking, increases the risk of formation of atherosclerotic plaques [18]. It is also evident from the literature that, the WSS distribution along the artery, is an important factor to predict the behavior of atherosclerosis disease [20-22]. Low shear stress increases the risk of formation and progression of atherosclerotic plaques in coronary arteries [23, 24]. In some studies, the WSS below 1 Pa is considered as low shear stress

Table 4. The location of stenosis and the average WSS over different regions along the artery with intermediate stenosis

Name	Model	Location of max stenosis centre from inlet (mm)	Average of WSS over proximal region (Pa)	Average of WSS over stenosis region (Pa)	Average of WSS over distal region (Pa)
Patient 8	Newtonian	79.3736	3.1354	7.9384	7.6596
	Carreau-Yasuda		3.1807	7.9675	7.6917
	Casson		3.2504	8.1910	7.9074
	Power-law		3.2727	7.2107	7.2418
Patient 9	Newtonian	40.5547	0.9805	2.9499	4.7666
	Carreau-Yasuda		1.0688	2.9971	4.7383
	Casson		1.1087	3.1140	4.8202
	Power-law		1.2641	2.9417	4.3689
Patient 10	Newtonian	30.7776	0.9658	1.8029	2.6201
	Carreau-Yasuda		1.0386	1.8428	2.6340
	Casson		1.0576	1.8760	2.7021
	Power-law		1.2075	1.8675	2.5053
Patient 11	Newtonian	45.9936	1.1348	1.6120	2.2853
	Carreau-Yasuda		1.1857	1.6302	2.2664
	Casson		1.2019	1.6597	2.3129
	Power-law		1.2909	1.6167	2.0806
Patient 12	Newtonian	11.8863	-	0.7518	2.2851
	Carreau-Yasuda		-	0.8327	2.2674
	Casson		-	0.8525	2.2974
	Power-law		-	0.9951	2.1634
Patient 13	Newtonian	93.1445	1.3245	4.1341	21.6291
	Carreau-Yasuda		1.4346	4.1740	21.3772
	Casson		1.5337	4.3377	22.3440
	Power-law		1.5427	3.9242	16.4969
Patient 14	Newtonian	83.4023	1.5413	2.2804	3.0706
	Carreau-Yasuda		1.5975	2.2328	3.0282
	Casson		1.6595	2.2002	3.0711
	Power-law		1.5963	2.2313	2.7599

[25]. However, high shear stress over lesion region may affect the plaque stability and lead to plaque rupture [23, 26].

Our findings showed that the pattern of dynamic viscosity is proportional to the size of coronary artery such that the smaller the artery the lower the dynamic viscosity (Figs. 10-12). Therefore, the average of dynamic viscosity in small arteries is less than medium and large arteries. It means that the possibility of plaque formation in small arteries is very low which is in agreement with the biological references [27, 28]. Similarity, the same conclusion can be obtained from the

average of WSS pattern along the arteries. It can be concluded from Figs. 10-12 that unlike the dynamic viscosity, the average of WSS in large arteries is less than small arteries which provides the better conditions to formation of atherosclerotic plaques. Because of the tapering nature of LAD arteries, in all cases the average of WSS over the proximal region was observed less than stenosis and distal regions. Similarity, earlier, it had been expressed by Johnston et al. (2004) [29] that the WSS at entrance to the right coronary artery (RCA) is less than the end of it. In some cases, the average of WSS

Table 5. The location of stenosis and the average WSS over different regions along the artery with severe stenosis

Name	Model	Location of Max Stenosis Centre From Inlet (mm)	Average of WSS over proximal region (Pa)	Average of WSS over stenosis region (Pa)	Average of WSS over distal region (Pa)
Patient 15	Newtonian	114.4326	8.0746	16.3097	-
	Carreau-Yasuda		8.1249	16.3660	-
	Casson		8.3284	16.9037	-
	Power-law		7.8325	14.4027	-
Patient 16	Newtonian	82.8713	4.8330	9.4849	6.5172
	Carreau-Yasuda		4.9026	9.4574	6.4682
	Casson		5.0668	9.4916	6.3685
	Power-law		4.6933	8.9323	5.9029
Patient 17	Newtonian	33.7708	2.8709	10.2732	7.9815
	Carreau-Yasuda		2.9369	10.3071	8.0597
	Casson		2.9916	10.5778	8.3032
	Power-law		3.2089	9.0221	7.5520
Patient 18	Newtonian	34.4772	0.6782	3.6016	4.8215
	Carreau-Yasuda		0.7673	3.6675	4.8366
	Casson		0.7843	3.8287	4.9263
	Power-law		0.9925	3.4434	4.5446
Patient 19	Newtonian	38.1156	0.7510	3.0825	4.5683
	Carreau-Yasuda		0.8463	3.1312	4.5970
	Casson		0.8881	3.2318	4.6922
	Power-law		1.0655	3.0518	4.3659
Patient 20	Newtonian	39.3299	1.9577	6.8641	2.4796
	Carreau-Yasuda		2.0680	6.8990	2.5450
	Casson		2.2188	7.1735	2.7165
	Power-law		1.9604	6.0469	2.3860

magnitude over proximal region is very low. For example, Fig. 7 shows the average of WSS over the proximal region using Newtonian, Carreau-Yasuda and Casson models, is less than 1 Pa. It expresses that, forming again of atherosclerotic plaques over proximal region is more probable than stenosis and distal regions.

Our results showed that the trend of variation of WSS and dynamic viscosity along particular artery are the same for all rheological models and there was a difference only in their magnitude. The contours of WSS and their percentage differences between Newtonian and non-Newtonian models showed that almost where the WSS range increased, the difference between rheological models decreased. It is true because over regions with high WSS range, the momentum has greater effect than the friction on blood flow through arteries and thus the importance of using viscosity model decreases. Based on our statistical

results, the WSS distribution resulted from different models, are approximately equal over the distal region (where the average of WSS is almost high) of each artery and there is no significant difference between them (Fig. 13). Since we used the cohort of patients with various stenosis sizes in our statistical analysis, we demonstrated that the conclusion discussed above is independent of the size of the lesion. Our results showed that in addition to WSS distribution over the distal segment, differences in the magnitude of maximum and minimum of shear stress and also their locations along each artery between various rheological models aren't statistically significant, too (Figs. 14-15). So even if the maximum and the minimum of WSS occur at distal region, the Newtonian model is still useful to simulating the blood flow in the artery over this region. For instance, to find the WSS distribution along the represented artery shown in Fig. 7 based on the Carreau-Yasuda model, it is enough
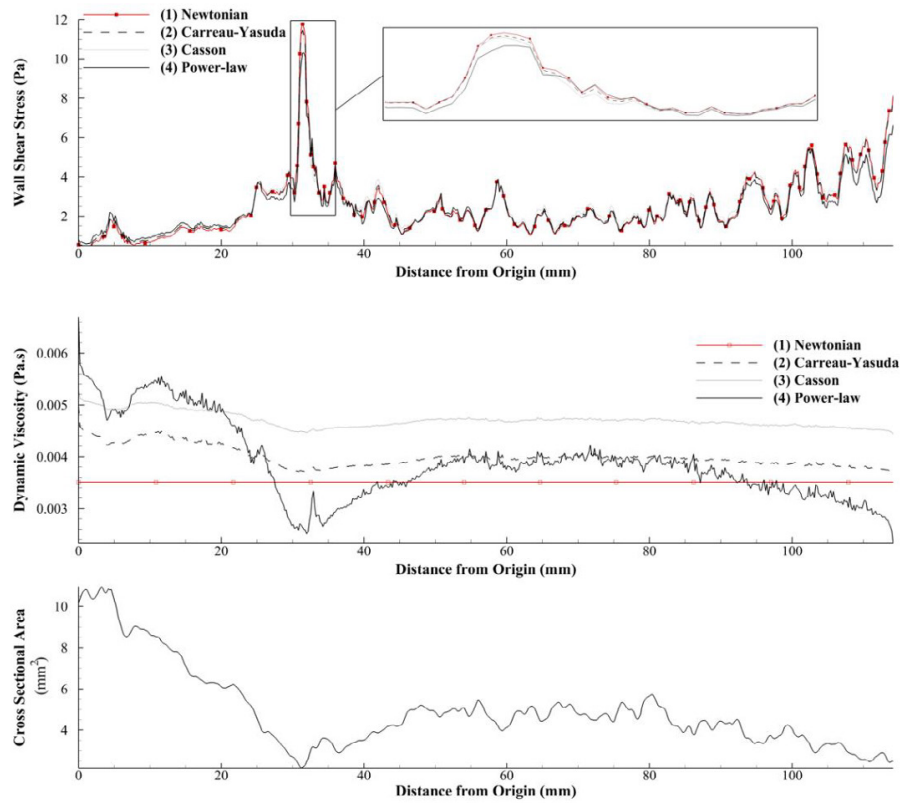
Fig. 10. Variation of the average of WSS, dynamic viscosity and cross-sectional area along the length of the artery for a representative patient with mild stenosis.
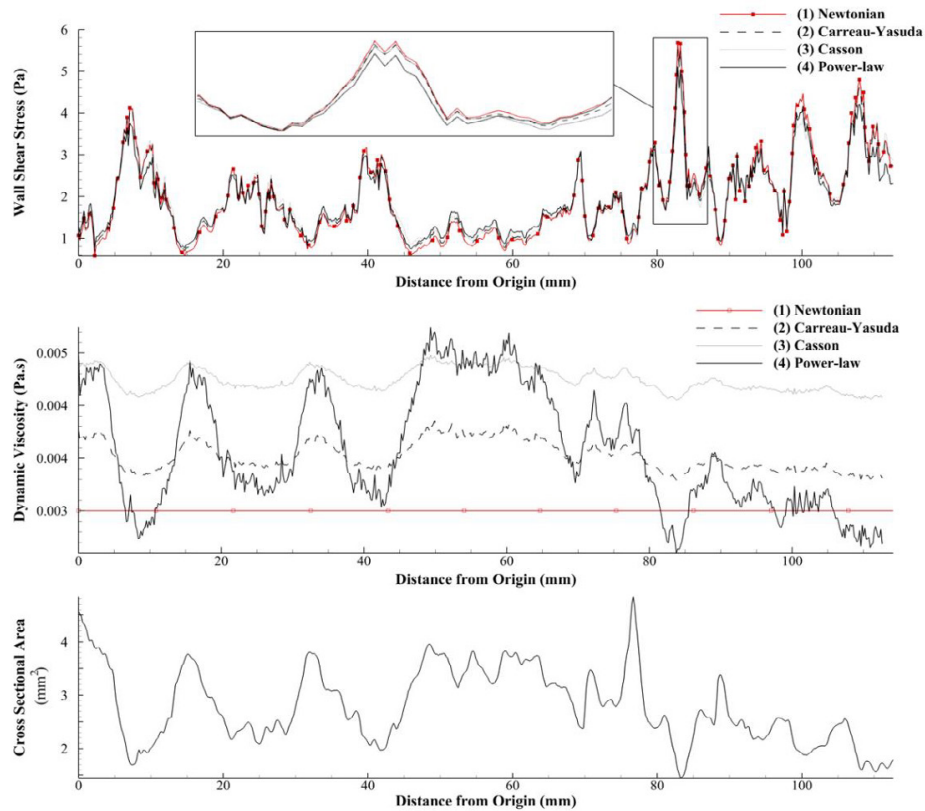

Fig. 11. Variation of the average of WSS, dynamic viscosity and cross sectional area along the length of the artery for a representative patient with intermediate stenosis.
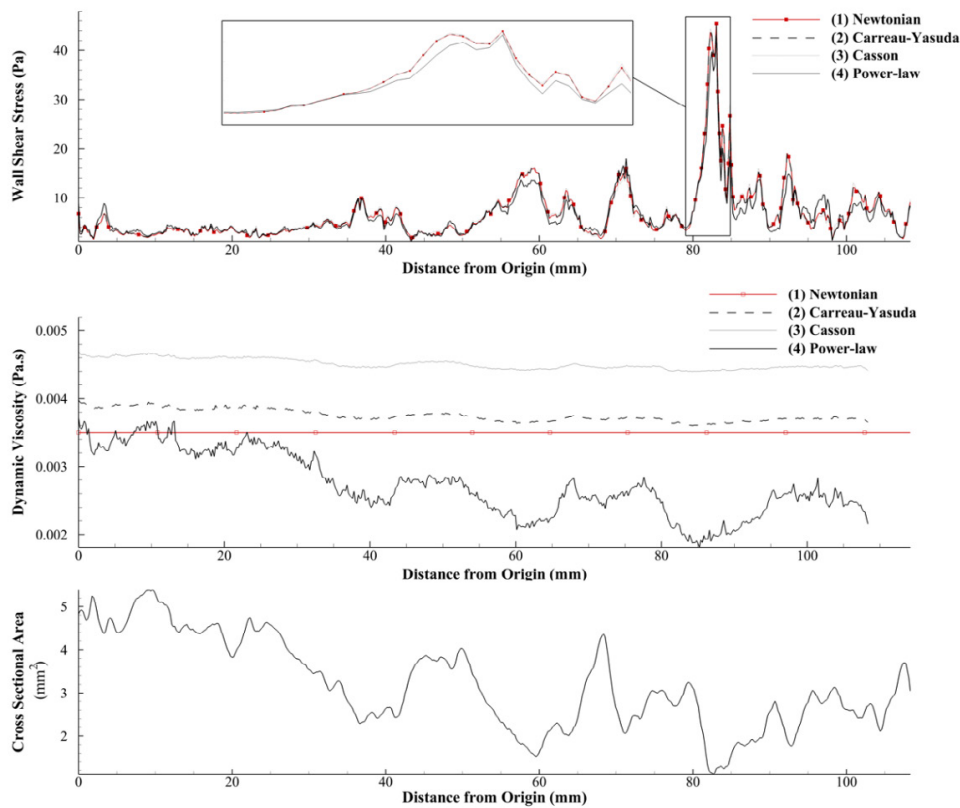
Fig. 12. Variation of the average of WSS, dynamic viscosity and cross-sectional area along the length of the artery for a representative patient with severe stenosis.

to simulate the first 50 mm of 115 mm long of the artery (regions (1) and (2)) using mentioned model. And to reduce the time of solution, we can simulate the remaining length of the artery using the Newtonian model instead of Carreau-Yasuda model. However, the results would be in a good agreement and there would not be a significant difference between them.

No research has been found that statistically examine the differences in WSS between Newtonian and non-Newtonian models to be compared with this work. However, this results are consistent with the findings of Johnston et al. (2004) [29]. They had shown that for regions of mid-range to high WSS, the Newtonian and non-Newtonian models are in good agreement.

4-1- Study limitations

In this study, the blood flow was considered the steady state. Due to the large number of case studies (20 patients x 4 models = 80 cases), simulation of these cases, regardless of this assumption, would be too time-consuming. Although this assumption affects the simulation results, since the purpose of this study is to compare the various viscosity models and not to determine the exact solution, the current results are acceptable. Also, previous studies have been shown that this assumption is reasonable for blood flow modeling in coronary arteries [30, 31].

In addition, the artery walls have been assumed to be

rigid and the effect of artery motion during the cardiac cycle has not been taken into account. This assumption has been shown to have no significant effect on simulation [32, 33].

5. Conclusions

The result showed that the average of WSS increased along the artery from proximal to distal regions. In all models, WSS distribution behaved in a similar manner along the artery, with increases associated with increasing arterial cross-sectional area and vice versa. Hence these results demonstrated the location of stenosis consistently. In addition, based on statistically analysis, there was no significant difference in WSS distribution over the distal region and also in maximum and minimum of it as well as their locations along each artery, between various models which can be helpful to reduce the run time process of simulation.

Acknowledgements

Nomenclature

u Velocity, m/s

p Pressure, Pa
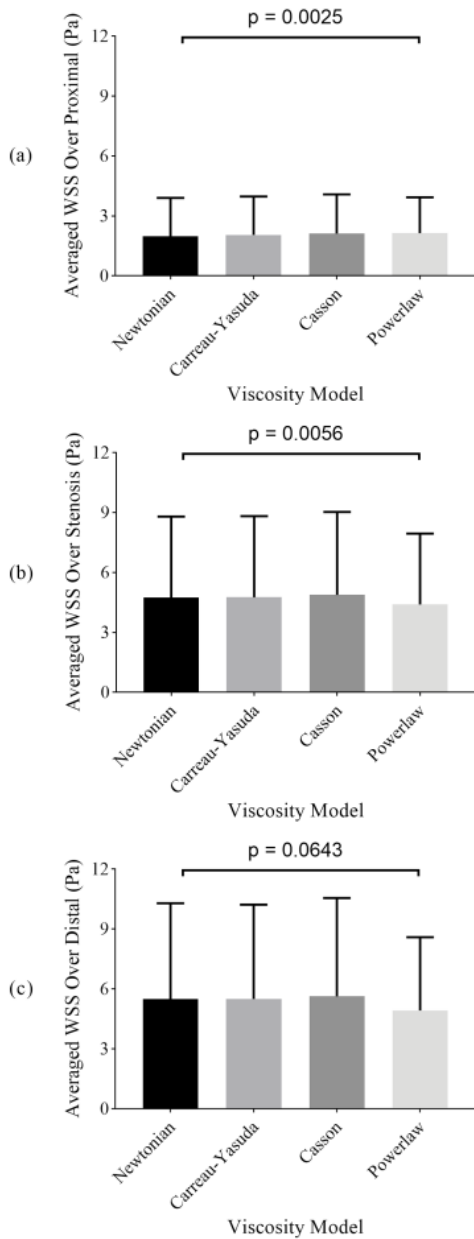
Greek symbols

Fig. 13. Comparison of the average of WSS between various blood viscosity models for the cohort of patients over (a) proximal region, (b) stenosis region and (c) distal region.

ρ Density, kg/m³
μ Dynamic viscosity, Pa.s
τ Shear stress, Pa

References

[1] S. Barquera, A. Pedroza-Tobías, C. Medina, L. Hernández-Barrera, K. Bibbins-Domingo, R. Lozano, A.E. Moran, Global Overview of the Epidemiology of Atherosclerotic Cardiovascular Disease, Archives of Medical Research, 46(5) (2015) 328-338.

[2] A. Javadzadegan, A. Moshfegh, H.H. Afrouzi, M. Omidi, Magnetohydrodynamic blood flow in patients with coronary artery disease, Computer Methods and Programs in Biomedicine, 163 (2018) 111-122.

[3] A. Javadzadegan, A. Moshfegh, M. Behnia, Effect of magnetic field on haemodynamic perturbations in atherosclerotic coronary arteries,
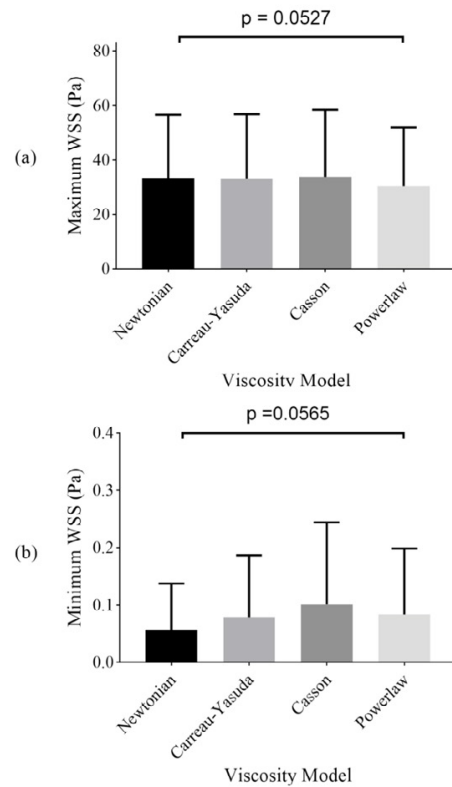
Fig. 14. Comparison of the (a) maximum and (b) minimum value of WSS along the artery between various blood viscosity models for the cohort of patients.
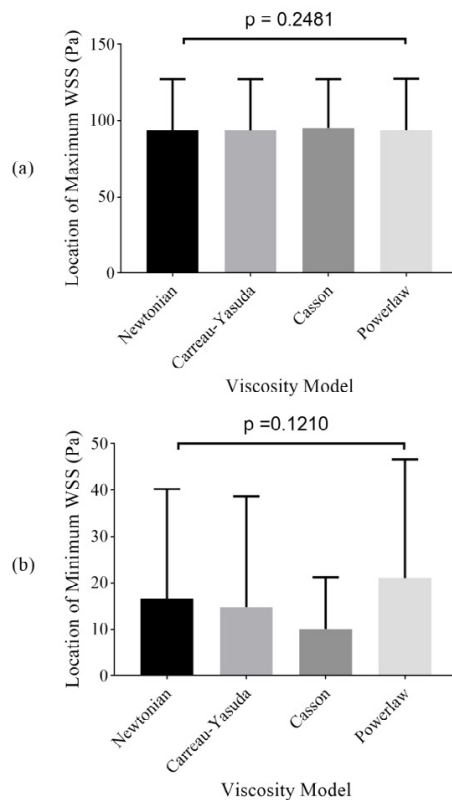

Fig. 15. Comparison of the location of (a) maximum and (b) minimum value of WSS along the artery between various blood viscosity models for the cohort of patients.

Journal of medical engineering & technology, 42(2) (2018) 148-156.

[4] S. Glagov, C. Zarins, D. Giddens, D. Ku, Hemodynamics and Atherosclerosis, Insights and perspectives gained from studies of human arteries, Archieves of Pathology and Laboratory Medicine 112 (1988) 1018–1031, C1016 References C1021 Author addresses, 1.

[5] L. Zhong, J.-M. Zhang, B. Su, R. San Tan, J.C. Allen, G.S. Kassab, Application of patient-specific computational fluid dynamics in coronary and intra-cardiac flow simulations: Challenges and opportunities, Frontiers in physiology, 9 (2018).

[6] R.A. Malinauskas, P. Hariharan, S.W. Day, L.H. Herbertson, M. Buesen, U. Steinseifer, K.I. Aycock, B.C. Good, S. Deutsch, K.B. Manning, FDA benchmark medical device flow models for CFD validation, ASAIO Journal, 63(2) (2017) 150-160.

[7] P.D. Morris, A. Narracott, H. von Tengg-Kobligk, D.A. Silva Soto, S. Hsiao, A. Lungu, P. Evans, N.W. Bressloff, P.V. Lawford, D.R. Hose, J.P. Gunn, Computational fluid dynamics modelling in cardiovascular medicine, Heart, 102(1) (2016) 18-28.

[8] S.A. Berger, L.-D. Jou, Flows in Stenotic Vessels, Annual Review of Fluid Mechanics, 32(1) (2000) 347-382.

[9] K. Perktold, M. Resch, H. Florian, Pulsatile Non-Newtonian Flow Characteristics in a Three-Dimensional Human Carotid Bifurcation Model, Journal of Biomechanical Engineering, 113(4) (1991) 464-475.

[10] D. Kumar, R. Vinoth, V.S. Raviraj Adhikari, Non-Newtonian and Newtonian blood flow in human aorta: a transient analysis, (2017).

[11] T.J. Pedley, The Fluid Mechanics of Large Blood Vessels, Cambridge University Press, 2008.

[12] F.J.H. Gijsen, F.N. van de Vosse, J.D. Janssen, The influence of the non-Newtonian properties of blood on the flow in large arteries: steady flow in a carotid bifurcation model, Journal of Biomechanics, 32(6) (1999) 601-608.

[13] D.S. Sankar, K. Hemalatha, A non-Newtonian fluid flow model for blood flow through a catheterized artery—Steady flow, Applied Mathematical Modelling, 31(9) (2007) 1847-1864.

[14] L. Goubergrits, E. Wellnhofer, U. Kertzscher, Choice and Impact of a Non-Newtonian Blood Model for Wall Shear Stress Profiling of Coronary Arteries, in, Springer Berlin Heidelberg, Berlin, Heidelberg, 2008, pp. 111-114.

[15] B.M. Johnston, P.R. Johnston, S. Corney, D. Kilpatrick, Non-Newtonian blood flow in human right coronary arteries: Transient simulations, Journal of Biomechanics, 39(6) (2006) 1116-1128.

[16] B. Liu, D. Tang, Influence of non-Newtonian properties of blood on the wall shear stress in human atherosclerotic right coronary arteries, Molecular & cellular biomechanics : MCB, 8(1) (2011) 73-90.

[17] Y. Jiang, J. Zhang, W. Zhao, Effects of the inlet conditions and blood models on accurate prediction of hemodynamics in the stented coronary arteries, AIP Advances, 5(5) (2015) 057109.

[18] K.R. Kensey, Y.I. Cho, M. Chang, Effects of Whole Blood Viscosity on Atherogenesis, The Journal of invasive cardiology, 9(1) (1997) 17-24.

[19] W.L. Siauw, E.Y.K. Ng, J. Mazumdar, Unsteady stenosis flow prediction: a comparative study of non-Newtonian models with operator splitting scheme, Medical Engineering & Physics, 22(4) (2000) 265-277.

[20] J. Suo, Y. Yan, J. Oshinski, A. Tannenbaum, J. Gruden, D. Giddens, Flow Patterns and Wall Shear Stress Distributions at Atherosclerotic-Prone Sites in a Human Left Coronary Artery - An Exploration Using Combined Methods of CT and Computational Fluid Dynamics, in: The 26th Annual International Conference of the IEEE Engineering in Medicine and Biology Society, 2004, pp. 3789-3791.

[21] J. Jung, A. Hassanein, R.W. Lyczkowski, Hemodynamic Computation Using Multiphase Flow Dynamics in a Right Coronary Artery, Annals of Biomedical Engineering, 34(3) (2006) 393.

[22] Y.H. Kim, P.J. VandeVord, J.S. Lee, Multiphase non-Newtonian effects on pulsatile hemodynamics in a coronary artery, International Journal for Numerical Methods in Fluids, 58(7) (2008) 803-825.

[23] V.A. Nosovitsky, O.J. Ilegbusi, J. Jiang, P.H. Stone, C.L. Feldman, Effects of Curvature and Stenosis-Like Narrowing on Wall Shear Stress in a Coronary Artery Model with Phasic Flow, Computers and Biomedical Research, 30(1) (1997) 61-82.

[24] Abdulrajak Buradi, A. Mahalingam, Numerical Simulation Of Pulsatile Blood Flow In An Idealized Curved Section Of A Human Coronary Artery, International Journal of Mechanical and Production Engineering (IJMPE), (Special Issue 2016) (2016) 15-19.

[25] W.-d. Qin, S.-h. Mi, C. Li, G.-x. Wang, J.-n. Zhang, H. Wang, F. Zhang, Y. Ma, D.-w. Wu, M. Zhang, Low shear stress induced HMGB1 translocation and release via PECAM-1/PARP-1 pathway to induce inflammation response, PLoS One, 10(3) (2015) e0120586.

[26] F. Gijsen, A. van der Giessen, A. van der Steen, J. Wentzel, Shear stress and advanced atherosclerosis in human coronary arteries, Journal of biomechanics, 46(2) (2013) 240-247.

[27] A.C. Guyton, J.E. Hall, Textbook of Medical Physiology, Elsevier Saunders, 2006.

[28] D.A. Cooley, G.W. He, Arterial Grafting for Coronary Artery Bypass Surgery, Springer Berlin Heidelberg, 2006.

[29] B.M. Johnston, P.R. Johnston, S. Corney, D. Kilpatrick, Non-Newtonian blood flow in human right coronary arteries: steady state simulations, Journal of Biomechanics, 37(5) (2004) 709-720.

[30] J. Soulis, G. Giannoglou, Y. Chatzizisis, T. M Farmakis, G. Giannakoulas, G. E Parcharidis, G. Louridas, Spatial and phasic oscillation of non-Newtonian wall shear stress in human left coronary artery bifurcation: An insight to atherogenesis, 2006.

[31] J.V. Soulis, G.D. Giannoglou, Y.S. Chatzizisis, K.V. Seralidou, G.E. Parcharidis, G.E. Louridas, Non-Newtonian models for molecular viscosity and wall shear stress in a 3D reconstructed human left coronary artery, Medical Engineering & Physics, 30(1) (2008) 9-19.

[32] R. Torii, N.B. Wood, N. Hadjiloizou, A.W. Dowsey, A.R. Wright, A.D. Hughes, J. Davies, D.P. Francis, J. Mayet, G.-Z. Yang, S.A.M. Thom, X.Y. Xu, Fluid–structure interaction analysis of a patient-specific right coronary artery with physiological velocity and pressure waveforms, Communications in Numerical Methods in Engineering, 25(5) (2009) 565-580.

[33] A. Santamarina, E. Weydahl, J.M. Siegel, J.E. Moore, Computational Analysis of Flow in a Curved Tube Model of the Coronary Arteries: Effects of Time-varying Curvature, Annals of Biomedical Engineering, 26(6) (1998) 944-954.